IL NUOVO CIMENTO **47 C** (2024) 272
DOI 10.1393/ncc/i2024-24272-y

COMMUNICATIONS: SIF Congress 2023

Design and realization of high-gradient C-band standing wave RF gun

F. CARDELLI(*)
INFN, Laboratori Nazionali di Frascati - Rome, Italy

received 22 January 2024

Summary. — To generate ultra-high brightness electron beams it is highly advantageous to use injectors based on Radio frequency photo-guns with very high cathode peak electric field. The current state of the art is the *S*-band (3 GHz) that allows to obtain cathode field at the level of 100 MV/m. To overcome the limits of this operating frequency a promising approach is to realize RF guns working at the C-band frequency (5712 MHz). In the context of the European I.FAST Project and INFN Commission V, a new *C*-band RF gun has been designed and realized at the INFN laboratories of Frascati. This RF gun has been fabricated with the brazing-free technology developed at the INFN and already applied to other electron sources. In this paper we present the design, the realization and the first tests performed on this prototype.

1. – Introduction

The EU has provided funding for the realization and testing of a *C*-Band photocaehode radiofrequency (RF) gun through the I.FAST Project [1], alongside support from INFN Commission V. The prospect of implementing a complete *C*-band injector is appealing due to its advantages in achievable beam parameters and compact design [2]. Moreover, the potential to operate at a high repetition rate, reaching up to 1 kHz, is a significant benefit. This is particularly relevant in the context of the *X*-band linacs within the EuPRAXIA@SPARC_LAB Project [3] and XLS CompactLight design study [4]. In general, this solution also holds great potential for applications in upgrading existing photo-injectors for Free Electron Lasers (FEL). The proposed RF gun is composed of 2.6 resonant cells operating in the π-*mode*. To reduce surface fields and improve mode frequency separation, it incorporates elliptical irises. To minimize pulsed heating and perfectly compensate for dipolar and quadrupolar components of the on-axis field, it

(*) E-mail: fabio.cardelli@lnf.infn.it

TABLE I. – *Main parameters of the C-band Gun (in parenthesis the measured ones).*

Parameter	Unit	Value
Resonant Frequency	MHz	5712 (5712)
$E_{cath}/\sqrt{P_{diss}}$	$\mathrm{MV/(m \cdot MW^{0.5})}$	51.4
RF input power	MW	18 (19)
Cathode peak field	MV/m	160
Rep. rate	Hz	100–400
Quality factor		11900 (11900)
Filling time	ns	166 (147)
Coupling coefficient		3 (3.5)
RF pulse length	ns	300
Mod. sep. $\pi - \pi/2$	MHz	47 (48.3)
E_{surf}/E_{cath}		0.96
Mod. Poy. vector	$W/\mu\mathrm{m}^2$	2.5
Pulsed heating	°C	16
Average diss. power	W	250–1000

uses a 4-port mode launcher as coupler. The electromagnetic design was conducted to achieve a high peak cathode field of 160 MV/m while maintaining a low breakdown rate using ultra-short RF pulses. To accomplish this, the coupling coefficient of the coupler was designed to be equal to 3. A previous article [5] details the electromagnetic design and sizing, as well as the thermal-mechanical analysis of the gun. The primary parameters resulting from these analyses are presented in table I.

Figure 1 provides the 3D mechanical layout of the initial part of the injector. Following the gun, there is an emittance compensating solenoid and a laser injection chamber facilitating laser injection with the last mirror in the air. Notably, the gun's construction avoids brazing, utilizing a new INFN-developed technology already applied in RF photoguns in the S-band frequency range [6, 7]. This innovative approach enables assembly the device in a clean room solely using screws with the use of special gaskets. Following assembly, vacuum testing and RF characterization are performed. A key advantage lies in the use of forged, non-annealed copper, which has demonstrated excellent performance in terms of conditioning time and breakdown rate, as confirmed by X-band high gradient tests [8] and our own assessments on S-band guns [6, 7]. The paper details the C-band gun's dark current simulations, the realization process and presents low-power RF measurement results. Additionaly, provides a brief explanation of the feeding scheme employed to power the gun without utilizing an isolator.

2. – Dark current simulations

For radiation protection reasons, it is crucial to assess the dark current generated by field emission from the surfaces exposed to the high fields generated within the gun. Two approaches, a theoretical one based on the Fowler-Nordheim (FN) emission model and a numerical one utilizing the 3D CST Particle-in-cell code, have been employed and compared to estimate the electrons field emitted from the cathode. The entire cathode surface has been considered as the particle source, and an emitter density factor has

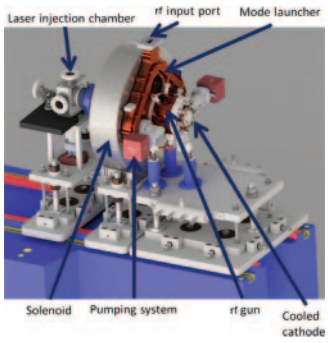

Fig. 1. – Mechanical Layout of the C-band Gun.

been introduced to scale the effective area of the emitters. The emitter area and the FN emission coefficient (β) characterize the entire emission process and depend largely on the cleanliness and roughness of the emitting surface, which are inherently unpredictable. To initiate a preliminary DC estimation, we adopted $\beta = 70$ and $A_e = 0.01\,\mu\text{m}^2$ as starting values for these parameters, evaluated at PSI for the SwissFEL Gun [9].

The Particle-in-cell (PIC) simulations, based on the methodology described in [10], incorporate the solenoid model to estimate the energy spectrum and the DC beam transport along the photo-injector up to the diagnostics chamber. The gun RF field and the solenoid's magnetic field were previously simulated with this geometry and then imported into the PIC simulations (fig. 2). Consequently, the transported charge at the laser injector chamber in an RF period, with a cathode peak field of 160 MV/m, was evaluated as 33 fC with the solenoid turned off and halved by turning on the solenoid. As a result of the simulations, the energy spectra of the dark current are shown in the fig. 2 for two different peak field values on the cathode.

3. – Gun components fabrication and assembly

The gun is a complex integration of various components, including standing wave (SW) cells, a four-port mode launcher, and the cathode. The mode launcher has been machined with a five-axis milling machine Micron UCP600 Vario, that ensures internal dimensions accuracy of $\pm 8\,\mu$m and surface roughness below 200 nm. Subsequently, it un-

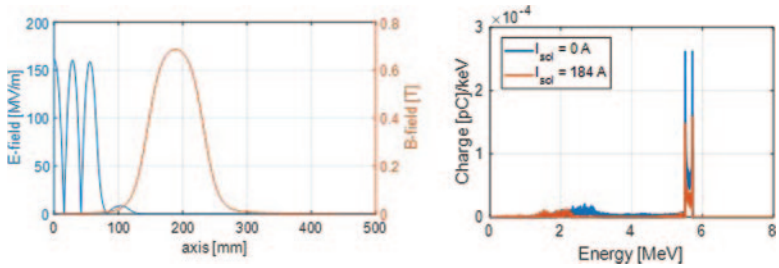

Fig. 2. – Amplitude of the electric and magnetic field on the gun axis (left) and dark current beam energy spectrum calculated with CST (right).

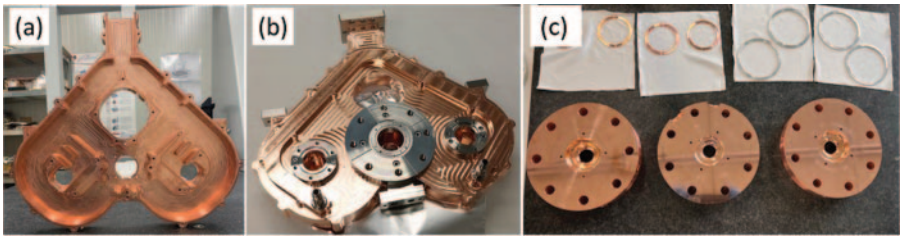

Fig. 3. – Machined mode launcher before (a) and after (b) brazing and standing wave copper cells (c).

dergoes vacuum brazing using palcusil 5 alloy, with fig. 3 showing the machined launcher before and after brazing process. RF test follows the vacuum testing of the brazed mode launcher. Standing wave cells and the cathode undergo machining on the lathe Schaublin 225 TM-CNC, achieving internal dimensions precision of $\pm 2\,\mu$m and surface roughness below 30 nm. After the machining, the cells have been cleaned using a bath of Almeco, followed by an NGL cleaning at 50 °C and a final treatment in citric acid to remove the oxidations. The cleaning procedure culminate in a vacuum furnace heating at 200 °C for 2 hours to remove residual water.

The final assembly is outlined in fig. 4. During the procedure the gun has been flushed with nitrogen and two kinds of special gaskets have been used to clamp each cell. An aluminum one, placed externally, for vacuum sealing and an internal copper gasket for RF contact. Alignment during assembly employs special "V" precise tools (fig. 4), ensuring proper cell alignment. Vacuum testing post-assembly, performed with a sensitivity below $1 \cdot 10^{-11}$ mbar/l/s, demonmstrate the gun sealing. Mechanical characterization of the assembled gun utilizes a CMM ALTERA 10.7.7, confirming cell alignment below $\pm 40\,\mu$m in both planes.

4. – RF Gun results

The assembled gun underwent RF testing using a network analyzer R&S ZVB 20, with measurements conducted under a nitrogen flux. The reflection coefficient at the input port is depicted in fig. 5, where the three modes are clearly discernible. The operational frequency, quality factor, and coupling coefficient, derived from fitting the reflection coefficient, are summarized in table I. Notably, the frequency and quality factor of the

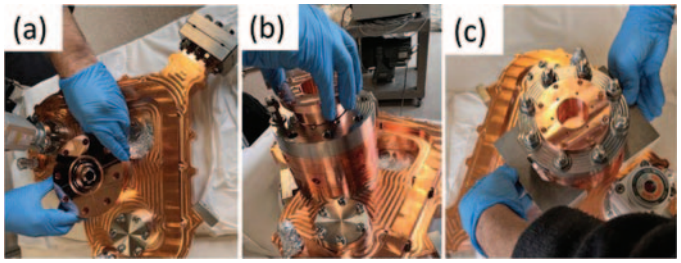

Fig. 4. – Assembly procedure of the gun: (a) cell assembly, (b) cathode insertion and (c) cell alignment before final clamping.

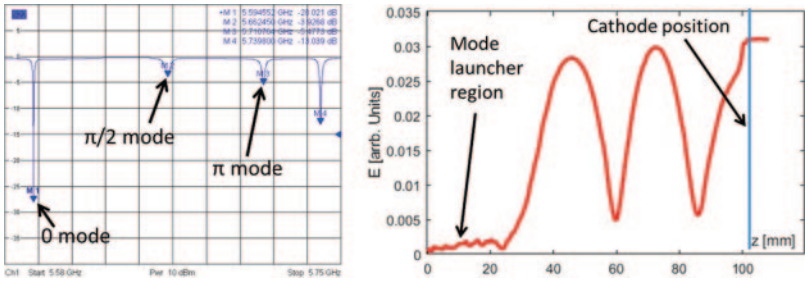

Fig. 5. – Reflection coefficient at the Gun input port (left) and Electric field profile on the Gun axis measured with the bead-drop technique.

working mode align with nominal values, while the coupling coefficient slightly exceeds expectations. Ongoing investigations are delving into the causes of this discrepancy, likely associated with the differing dimensions of the first coupling iris. Nonetheless, this variance in the coupling coefficient has negligible effects on gun performance in terms of required power, RF pulse length, and cathode peak field.

To assess the electric field on the axis, a metallic bead (2 mm diameter) connected to a nylon wire was dropped into the gun, yielding the results in fig. 5. The field imbalance between cells is approximately 5%. Unfortunately, the bead drop technique cannot measure the cathode peak field at the cathode plane due to the impact of image currents on the measurement. However, extrapolation by local fit indicates a cathode position field comparable to that on the first cell, approximately 5% below the central one. Ongoing investigations focus on understanding the reasons for this discrepancy with respect to the ideal simulated value, potentially attributing it to small deformations in the special copper gaskets used for RF contact and tolerances in fabrication, which even at a few micrometers, can influence field flatness.

5. – Gun feeding scheme without isolator

The original gun feeding scheme initially foreseen the utilization of a new in-vacuum isolator. However, the delivery of this component encountered delays due to challenges experienced during its fabrication. To mitigate potential setbacks and to provide a

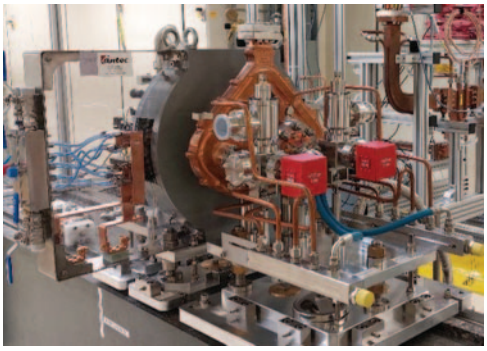

Fig. 6. – Picture of the gun assembled and installed in the PSI testing area.

contingency solution in case the new device fails to meet the required power performance, an alternative scheme was devised. This alternative approach employs power divider and a BOC-type pulse compressor, which is already available at PSI. The power from the klystron is divided using a 1:10 ratio power splitter and then compressed utilizing the pulse compressor. Subsequently, the reflected power from the cavity is split back with the same ratio. This devised scheme enables the attainment of a cathode peak field of 160 MV/m. Currently, the gun has been installed in the testing facility at PSI in Switzerland for the high-power test. Along with it, the waveguide feeding system, the pulse compressor, and the power splitter just described have also been installed. Figure 6 depicts the gun with its solenoid installed in the facility at PSI.

6. – Conclusion

At INFN-LNF, the recently developed C-band electron gun represents a significant advancement, featuring cutting-edge technology that eliminates the need for brazing during its design and fabrication. The gun has undergone several testing, including vacuum and low-power RF assessments, with the measured RF parameters demonstrating good alignment with expectations. Successfully integrated into the experimental setup for high-power testing, the gun's performance is now being evaluated as part of the I.FAST project at PSI. The high-power testing phase began in January 2024; it will verify the performances of the gun as anticipated during the design phase, demonstrating its effective functionality and reliability at high gradient.

* * *

The author would like to thank the entire INFN team that contributed to this work, especially D. Alesini, G. Di Raddo, L. Faillace, A. Gallo, A. Giribono, A. Gizzi, S. Lauciani, A. Liedl, L. Pellegrino, L. Piersanti, C. Vaccarezza and A. Vannozzi. Furthermore, the author would like to thank the COMEB company for the technical support in gun realization. This project has received funding from the European Union's Horizon 2020 Research and Innovation program under GA No.101004730 and from the INFN Commission V.

REFERENCES

[1] I.FAST Project, https://ifast-project.eu/home.
[2] Giribono A. *et al.*, *Phys. Rev. Accel. Beams*, **26** (2023) 083402.
[3] Ferrario M. *et al.*, *Nucl. Instrum. Methods A*, **909** (2018) 134.
[4] Compact Light, http://www.compactlight.eu/Main/HomePage.
[5] Alesini D. *et al.*, *The new c band gun for the next generation rf photo-injectors*, in *Proceedings of IPAC22, 2022, Bangkok, Thailand* (JACoW) 2022, https://doi.org/10.18429/JACoW-IPAC2022-MOPOMS021.
[6] Shpakov V. *et al.*, *J. Instrum.*, **17** (2022) 12022.
[7] Alesini D. *et al.*, *Phys. Rev. Accel. Beams*, **21** (2018) 112001.
[8] Simakov E., Doplgashev V. A. and Tantawi S. G., *Nucl. Instrum. Methods Phys. Res. Sect. A*, **907** (2018) 221.
[9] Bettoni S. *et al.*, *Phys. Rev. Accel. Beams*, **21** (2018) 023401.
[10] Cardelli F. *et al.*, *Dark current studies for a high gradient SW C-band RF Gun*, in *Proceedings of IPAC22, 2022, Bangkok, Thailand* (JACoW) 2022, https://doi.org/10.18429/JACoW-IPAC2022-MOPOMS020.